ELSEVIER

Engineering Analysis with Boundary Elements 23 (1999) 671–681

ENGINEERING ANALYSIS *with* BOUNDARY ELEMENTS

www.elsevier.com/locate/enganabound

Closed-form integration of singular terms for constant, linear and quadratic boundary elements. Part 1. SH wave propagation

A.J.B. Tadeu[a,*], P.F.A. Santos[a], E. Kausel[b]

[a]*Department of Civil Engineering, University of Coimbra, 3020 Coimbra, Portugal*
[b]*Department of Civil and Environmental Engineering, Massachusetts Institute of Technology, Cambridge, MA 02139, USA*

Received 27 November 1998; accepted 11 May 1999

Abstract

One of the most important aspects in the application of boundary element techniques to wave propagation problems is the accurate representation of the singular terms at the points of application of the virtual loads. It is current practice to carry out this task by means of numerical quadrature. This paper presents an *analytical* evaluation of the singular integrals for constant, linear and quadratic boundary elements involving SH waves, the results of which are then used to model inclusions in a two-dimensional acoustic medium illuminated by dynamic anti-plane line sources. Finally, the BEM results are compared with the known analytical solutions for cylindrical inclusions.

Keywords: Wave propagation; Shear waves; Elastic inclusions; Scattering; Boundary element method; Singular integrals

1. Introduction

Studies on the effects of geologic and topographic irregularities on wave propagation in soil media have been motivated primarily by the need to better understand the spatial variation and intensity of seismic motions. Among the objectives of these studies are the effects that alluvial basins [1] and obstacles in the path of waves, such as cavities [2], have on seismic motions in their vicinity, and which are caused by wave diffraction, scattering and reverberations. The tools used to analyse these problems range from the semi-analytical methods applied by Lee [3] to study wave diffraction near geological irregularities, to purely numerical methods, such as finite elements combined with transmitting boundaries. The latter have been mostly restricted to situations where the response is required only in localised irregular domains, such as for soil structure interaction problems [4]. Discrete methods have also been used to model large alluvial basins, but for the most part only in plane-strain. Finally, hybrid methods that involve a combination of finite elements to model the inhomogeneous interior domain, and semi-analytical representations for the exterior domain, have been used by Sanchez-Sesma [5].

Possibly the best means of analysing wave propagation problems in unbounded media is the boundary element method (BEM), because it automatically satisfies the far field radiation conditions and allows a compact description of the medium in terms of boundary elements at the material discontinuities only. As is well known, the BEM is based on the use of appropriate fundamental solutions, or Green's functions, relating the field variables (stresses, displacements) in a homogeneous medium to point sources placed somewhere in the medium. The fundamental solution most often used is that of an infinite homogeneous space, because it is known in closed-form and has a relatively simple structure. However, BEMs based on the Green's functions for a half-space have also been used to solve several problems involving diffraction of waves by surface irregularities of arbitrary shape [6,7], as well as for cavities and buried structures [8].

A very important aspect in the application of boundary element techniques to wave propagation problems is the accurate representation of the singular terms at the points of application of the virtual loads [9–12]. To improve on the current state of practice, which relies exclusively on numerical integration, this paper first presents an analytical evaluation of the singular integrals for constant, linear and quadratic boundary elements formulated in the frequency domain. These analytical expressions are then validated by means of a Gauss–Legendre numerical quadrature, and thereafter, the formulae are applied to an example of wave scattering by cylindrical *inclusions* in a homogeneous, two-dimensional acoustic medium when illuminated by dynamic anti-plane line sources. Finally, the BEM results are

* Corresponding author.

0955-7997/99/$ - see front matter
PII: S0955-7997(99)00016-8

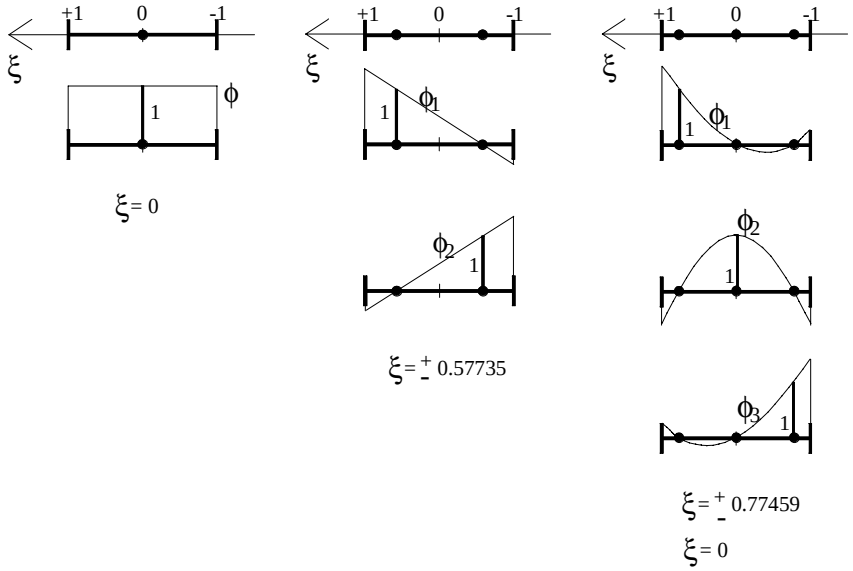

Fig. 1. Interpolation functions and position of the Gauss–Legendre nodes.

compared with the analytical solutions for these problems presented by Pao and Mow [13].

2. Boundary element formulation

The fundamental equations underlying the application of boundary elements to wave propagation are certainly well known (for example, see Manolis [14]). Thus, it suffices to state here that application of the method requires integration of the Green's functions, and of their derivatives, for all elements used to model the problem at hand:

$$H_{33}^{kl} = \int_{C_l} \phi H_{33}(x_k, x_l, n_l)\, \mathrm{d}C_l \tag{1}$$

$$G_{33}^{kl} = \int_{C_l} \phi G_{33}(x_k, x_l)\, \mathrm{d}C_l \tag{2}$$

in which $G_{33}(x_k, x_l)$ and $H_{33}(x_k, x_l, n_l)$ are, respectively, the components of the Green's tensor for displacement and traction components at x_k due to a concentrated load at x_l; n_l is the unit outward normal for the lth boundary segment C_l, and ϕ is an interpolation function. In the case of a medium under plane-strain conditions subjected to anti-plane line loads, the required Green's function is:

$$G_{33}(x, x_0) = \mathrm{i}/(4\mu)\; H_0(k_\beta r) \tag{3}$$

In this equation μ is the Lamé constant; $k_\beta = \omega/\beta$ is the wave-number; ω is the circular frequency; $\beta = \sqrt{\mu/\rho}$ is the velocity of shear waves; ρ is the mass density; $r = |x - x_0|$ is the source–receiver distance; $H_n(\,) = H_n^{(2)}$ is the Hankel function of the second kind of order n, and $\mathrm{i} = \sqrt{-1}$.

The variations of displacement and stresses within an element are controlled by the interpolation function used to map the nodal values for these quantities. In addition, the different slopes at the junction of two contiguous elements also play a role in the computation of the stress resultants. In this work, the writers use discontinuous elements to allow nodal points in which only the stresses relative to the element itself are considered. To enhance the accuracy of the results, the nodal points are chosen to coincide with those in a Gauss–Legendre numerical integration (Fig. 1). This issue is discussed further in a companion paper [15].

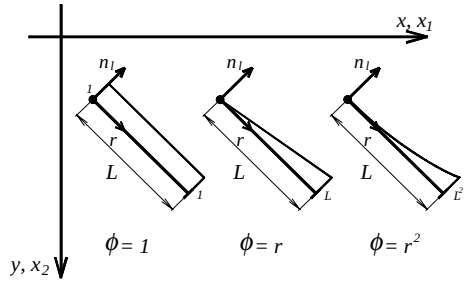

Fig. 2. Local co-ordinate system for segment integration.

3. Element integration

When the element to be integrated in Eqs. (1) and (2) is not the loaded element, the integrands are non-singular and the integration is best carried out using Gaussian quadrature. For the loaded element, however, the integrands exhibit a singularity, but it is then possible to carry out the integration in closed form, as will be shown.

To demonstrate this assertion, consider the singular segment of length L shown in Fig. 2, which represents, constant, linear and quadratic functions. Since in this case r is perpendicular to the normal (i.e. $rn_l = 0$), the singular term H_{33}^{ll} disappears. However, the integration of the

Green's function G_{33}^{ll} for constant, linear and quadratic elements involves evaluation of the three expressions

$$\int_0^L H_0(k_\beta r)\,\mathrm{d}r; \qquad \int_0^L rH_0(k_\beta r)\,\mathrm{d}r; \qquad \int_0^L r^2 H_0(k_\beta r)\,\mathrm{d}r \tag{4}$$

Integration of $\int_0^L H_0(k_\beta r)\,\mathrm{d}r$.

This integral follows directly from the expressions in Abramowitz [16] (pp. 480, eq. 11.1.7),

$$\int_0^L H_0(k_\beta r)\,\mathrm{d}r = \int_0^L [J_0(k_\beta r) - \mathrm{i}\,Y_0(k_\beta r)]\,\mathrm{d}r$$

$$= L[I_1(b) - \mathrm{i}\,I_2(b)] \tag{5}$$

in which $b = k_\beta L$ is the dimensionless wave-number, and

$$I_1(b) = J_0(b) + \frac{\pi}{2}[S_0(b)J_1(b) - S_1(b)J_0(b)]$$

$$I_2(b) = Y_0(b) + \frac{\pi}{2}[S_0(b)Y_1(b) - S_1(b)Y_0(b)]$$

Here $S_0(\,)$ and $S_1(\,)$ are Struve functions while $J_n(\,)$ and $Y_n(\,)$ are nth order Bessel functions of the first and second kind, respectively.

Integration of $\int_0^L rH_0(k_\beta r)\,\mathrm{d}r$.

This integral uses once more the expressions in Abramowitz [16] (pp. 484, eq. 11.3.20 and eq. 11.3.24),

$$\int_0^L rH_0(k_\beta r)\,\mathrm{d}r = \int_0^L r[J_0(k_\beta r) - \mathrm{i}\,Y_0(k_\beta r)]\,\mathrm{d}r$$

$$= I_3(b) - \mathrm{i}\,I_4(b) \tag{6}$$

with $b = k_\beta L$, and

$$I_3(b) = \left[\frac{L}{k_\beta} J_1(b)\right]$$

$$I_4(b) = \left[\frac{L}{k_\beta} Y_1(b) + \frac{2}{\pi k_\beta^2}\right]$$

Integration of $\int_0^L r^2 H_0(k_\beta r)\,\mathrm{d}r$.

Making use of the recurrence relation for the Bessel functions

$$\frac{r^2}{k_\beta}\frac{\mathrm{d}H_1(k_\beta r)}{\mathrm{d}r} = -\frac{r}{k_\beta}H_1(k_\beta r) + r^2 H_0(k_\beta r) \tag{7}$$

one obtains

$$\int_0^L r^2 H_0(k_\beta r)\,\mathrm{d}r = \int_0^L \frac{r}{k_\beta}H_1(k_\beta r)\,\mathrm{d}r + \int_0^L \frac{r^2}{k_\beta}\frac{\mathrm{d}H_1(k_\beta r)}{\mathrm{d}r}\mathrm{d}r \tag{8}$$

Integrating by parts, these integrals may be written as

$$\frac{1}{k_\beta}\int_0^L rH_1(k_\beta r)\,\mathrm{d}r$$

$$= \lim_{\varepsilon\to 0}\left[-\frac{r}{k_\beta^2}H_0(k_\beta r)\right]_\varepsilon^L + \frac{1}{k_\beta^2}\int_0^L H_0(k_\beta r)\,\mathrm{d}r \tag{9}$$

$$\int_0^L \frac{r^2}{k_\beta}\frac{\mathrm{d}H_1(k_\beta r)}{\mathrm{d}r}\mathrm{d}r$$

$$= \lim_{\varepsilon\to 0}\left[\frac{r^2}{k_\beta}H_1(k_\beta r)\right]_\varepsilon^L - \frac{2}{k_\beta}\int_0^L rH_1(k_\beta r)\,\mathrm{d}r \tag{10}$$

Hence,

$$\int_0^L r^2 H_0(k_\beta r)\,\mathrm{d}r = -\frac{1}{k_\beta^2}\int_0^L H_0(k_\beta r)\,\mathrm{d}r$$

$$+ \lim_{\varepsilon\to 0}\left[\frac{1}{k_\beta}\left(\frac{r}{k_\beta}H_0(k_\beta r) + r^2 H_1(k_\beta r)\right)\right]_\varepsilon^L \tag{11}$$

It may be observed that Eq. (11) contains two indeterminate expressions, namely $\lim_{\varepsilon\to 0}[rY_0(k_\beta r)]_\varepsilon = 0\times\infty$ and $\lim_{\varepsilon\to 0}[r^2 Y_1(k_\beta r)]_\varepsilon = 0\times\infty$. However, by considering the ascending series for the Bessel functions Y_0, Y_1 (Abramowitz [16], pp. 480, eq. 9.1.11 and eq. 9.1.13), it may be concluded that

$$\lim_{\varepsilon\to 0}[rY_0(k_\beta r)]_\varepsilon \cong \lim_{\varepsilon\to 0}\frac{2}{\pi}\left[r\ln\left(\frac{k_\beta r}{2}\right) + \gamma r\right]_\varepsilon = 0 \tag{12}$$

and

$$\lim_{\varepsilon\to 0}[r^2 Y_1(k_\beta r)]_\varepsilon \cong \lim_{\varepsilon\to 0}\left[-\frac{r^2}{\pi}\Gamma(1)\left(\frac{1}{2}k_\beta r\right)^{-1}\right]_\varepsilon = 0 \tag{13}$$

where γ is Euler's constant. This leads in turn to

$$\int_0^L r^2 H_0(k_\beta r)\,\mathrm{d}r = -\frac{1}{k_\beta^2}\int_0^L H_0(k_\beta r)\,\mathrm{d}r$$

$$+ \frac{1}{k_\beta}\left(\frac{L}{k_\beta}H_0(b) + L^2 H_1(b)\right) \tag{14}$$

with $b = k_\beta L$. Notice that $J_0(0) = 1$, $J_1(0) = 0$, and $\lim_{\varepsilon\to 0}[x\ln x]_\varepsilon = 0$. Also, the first term in Eq. (14) is provided by Eq. (5).

4. Analytical versus numerical integration

The analytical expressions described previously are next implemented and compared with the results obtained by means of the Gauss–Legendre quadrature. The integrals $\int_0^L H_0(k_\beta r)\,\mathrm{d}r$; $\int_0^L rH_0(k_\beta r)\,\mathrm{d}r$; $\int_0^L r^2 H_0(k_\beta r)\,\mathrm{d}r$ are computed along a straight line, using two, four and six integration points. Computations are performed in the

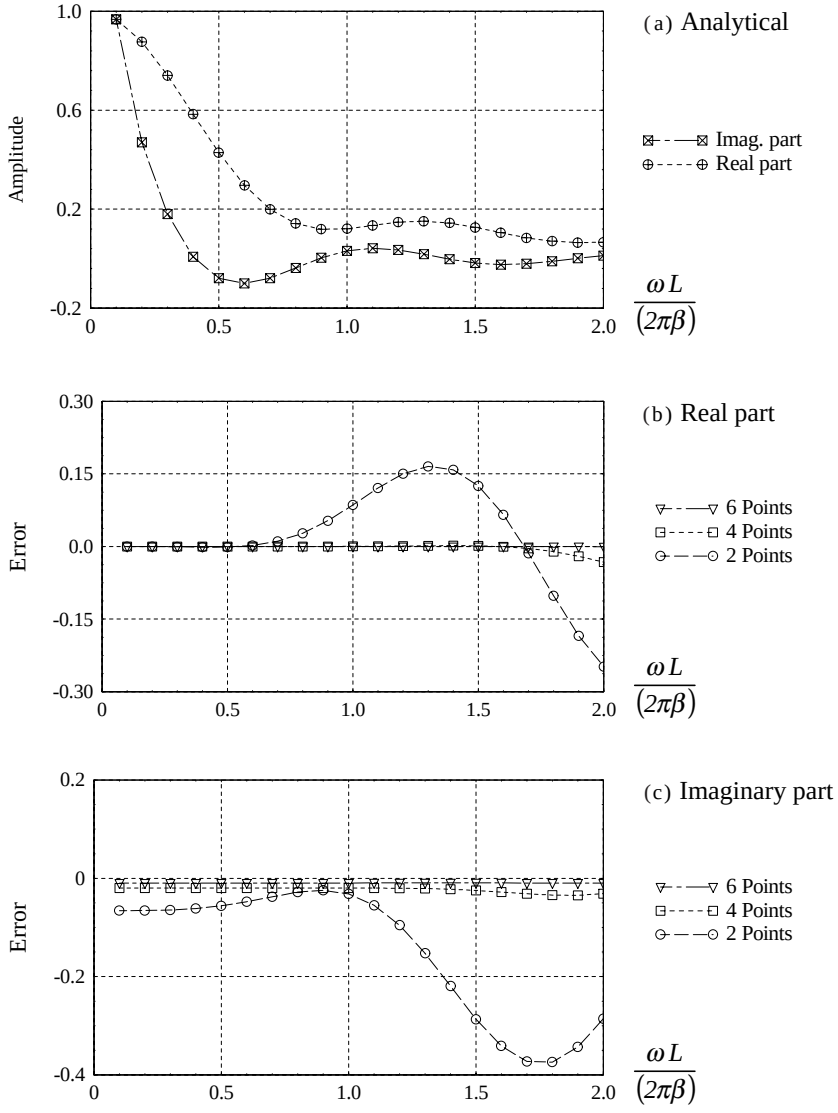

Fig. 3. Integration of $\int_0^L H_0(k_\beta r)\,\mathrm{d}r$.

frequency range [10, 200 Hz] at increments of 10 Hz. Also, the shear wave velocity and the element length L are assumed to be 100 m/s and 1.0 m, respectively.

Figs. 3(a), 4(a) and 5(a) show the results for the three integrals obtained with the analytical and numerical integration methods in terms of the excitation frequency. However, Figs. 3(b) and (c), 4(b) and (c), 5(b) and (c) illustrate the relative errors introduced by numerical quadrature. As expected, the accuracy of the numerical integration improves with the number of Gaussian points, and is virtually exact at the highest resolution of six points. By contrast, the errors in the numerical quadrature are substantial when using only two integration points.

These findings suggest that a purely numerical solution with an adequate number of integration points can be satisfactory from a computational point of view, even if the analytical expressions involve less uncertainty. Still, the exact solution could be useful as a benchmark, allowing the testing of programs for errors, even when opting for a purely numerical model.

5. Example of application

The method and expressions described above are next applied to the problem of a cylindrical inclusion buried in an infinite homogeneous space. Two inclusions are considered, namely a cavity and an elastic cylinder. Both are illuminated by shear (SH) waves elicited by an anti-plane source that is parallel to the axis of the cylinder. The cylindrical incident field is given by $u_3^{\mathrm{inc}} = (H_0 k_{\beta 1} r)$, where $k_{\beta 1} = \omega/\beta_1$ is the wave-number; ω is the circular frequency; β_1 is the velocity of shear waves in the medium surrounding the inclusion, and r is the source–receiver distance. The receiver registering the response is placed as shown in Fig. 6.

In a first test, the elastic inclusion is assigned the same

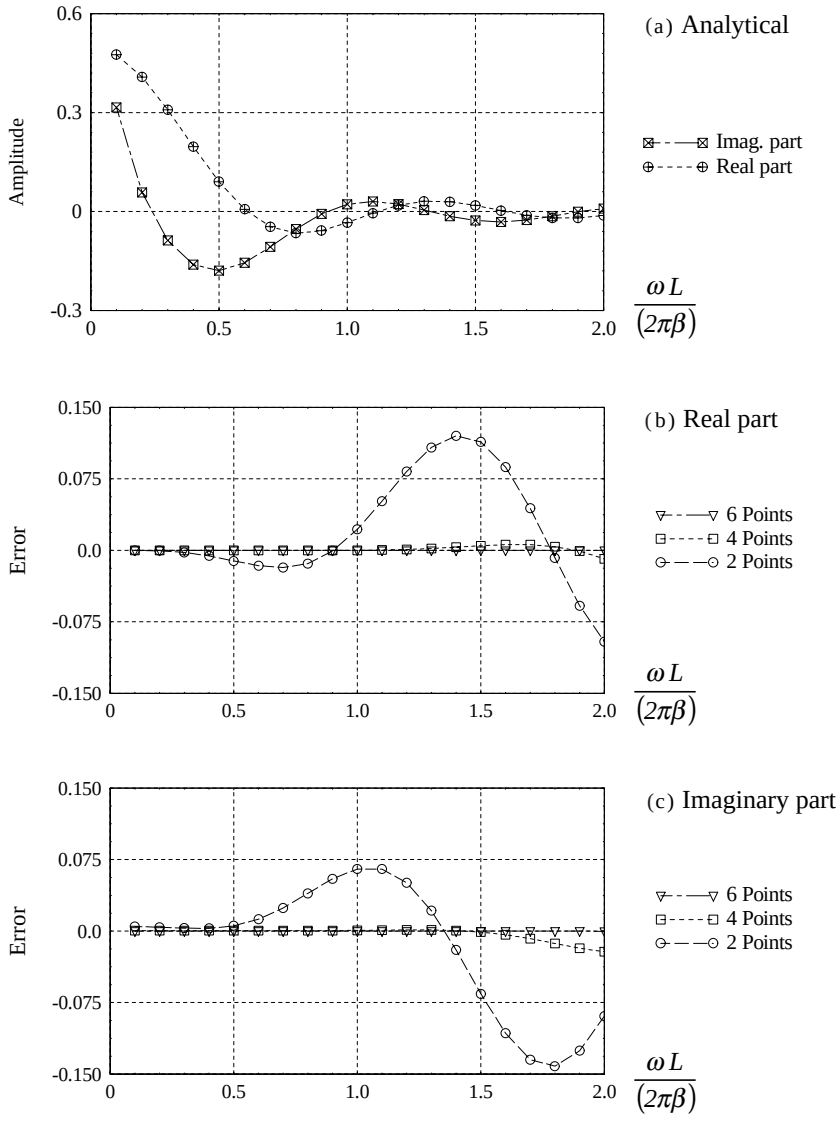

Fig. 4. Integration of $\int_0^L rH_0(k_\beta r)\,\mathrm{d}r$.

material properties as the surrounding medium; as expected, this test reproduces the free field conditions. The program is subsequently tested with the material properties shown in Fig. 6. In these analyses, 64 frequencies in the range from 1 to 64 Hz are considered. These frequencies imply SH waves whose wavelengths range between 10 and 0.156 times the diameter of the cylinder. The response at the receiver station is evaluated both in closed form [13] and by using the BEM program implementing the analytical integration of the singular terms. In the latter case, the computation is carried out using constant, linear and quadratic elements. To illustrate the effect of nodal spacing on the response functions, the number of elements is varied between 5 and 50.

Figs. 7–10 give the results for a cavity. Figs. 7 and 8 show the response (real part, imaginary part and modulus) at the receiver station for a cavity modelled, respectively, with 25 and 50 elements. As expected, the BEM accuracy is much greater at low frequencies than at high frequencies. The reason is, of course, that high frequencies involve short wavelengths, so shorter boundary elements are needed to appropriately model the response. In the present example, the ratio between the wavelength of the incident waves to the length of boundary elements ranges from 15.92 to 159.23 for a frequency of 1 Hz and from 0.249 to 2.49 for a frequency of 64 Hz. It can further be observed that linear elements outperform constant elements with results closer to the analytical solution. Quadratic elements, in turn, are better than linear elements, because they are better able to model variations in displacements and/or tractions.

Figs. 9 and 10 show the absolute value of the scattered field when the cavity is modelled with 5 to 50 elements, for a

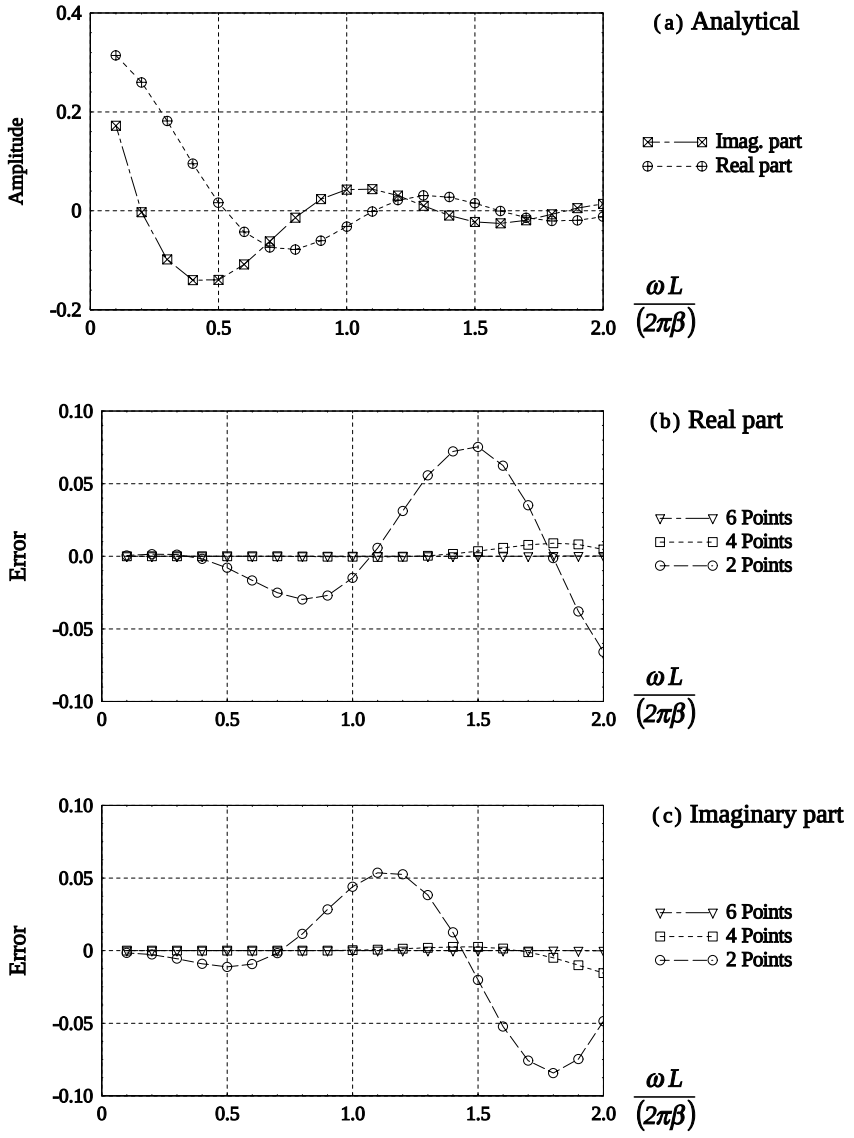

Fig. 5. Integration of $\int_0^L r^2 H_0(k_\beta r)\,\mathrm{d}r$.

source whose frequency varies between 32 (Fig. 9) and 64 Hz (Fig. 10). This range corresponds to incident waves with wavelengths of 6.25 and 3.125, respectively. Once more, the solution is seen to improve with the number of boundary elements and with changes from constant to linear to quadratic elements.

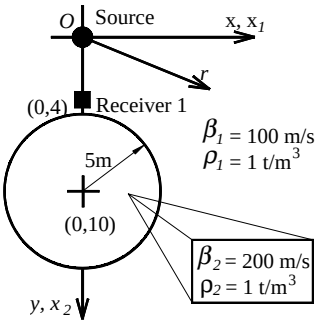

Fig. 6. Cylindrical inclusion in an unbounded medium.

Figs. 11–14 illustrate the response obtained for the case of an elastic inclusion similar in size and shape to the cavity. While the response again improves with the number of nodes and the refinement in the boundary elements used, a higher number of nodes per element is not necessarily beneficial, because of the increased computational expense that these more accurate models entail. Indeed, a balance can be struck between the number and type of elements used. The more precise and expensive quadratic elements could be advantageous when calculating responses at points of rapidly changing states of stress and deformation. These can be expected to occur in the neighbourhood of heterogeneities or sharp discontinuities in geometry and material properties in the medium, such as corners of the elastic inclusion.

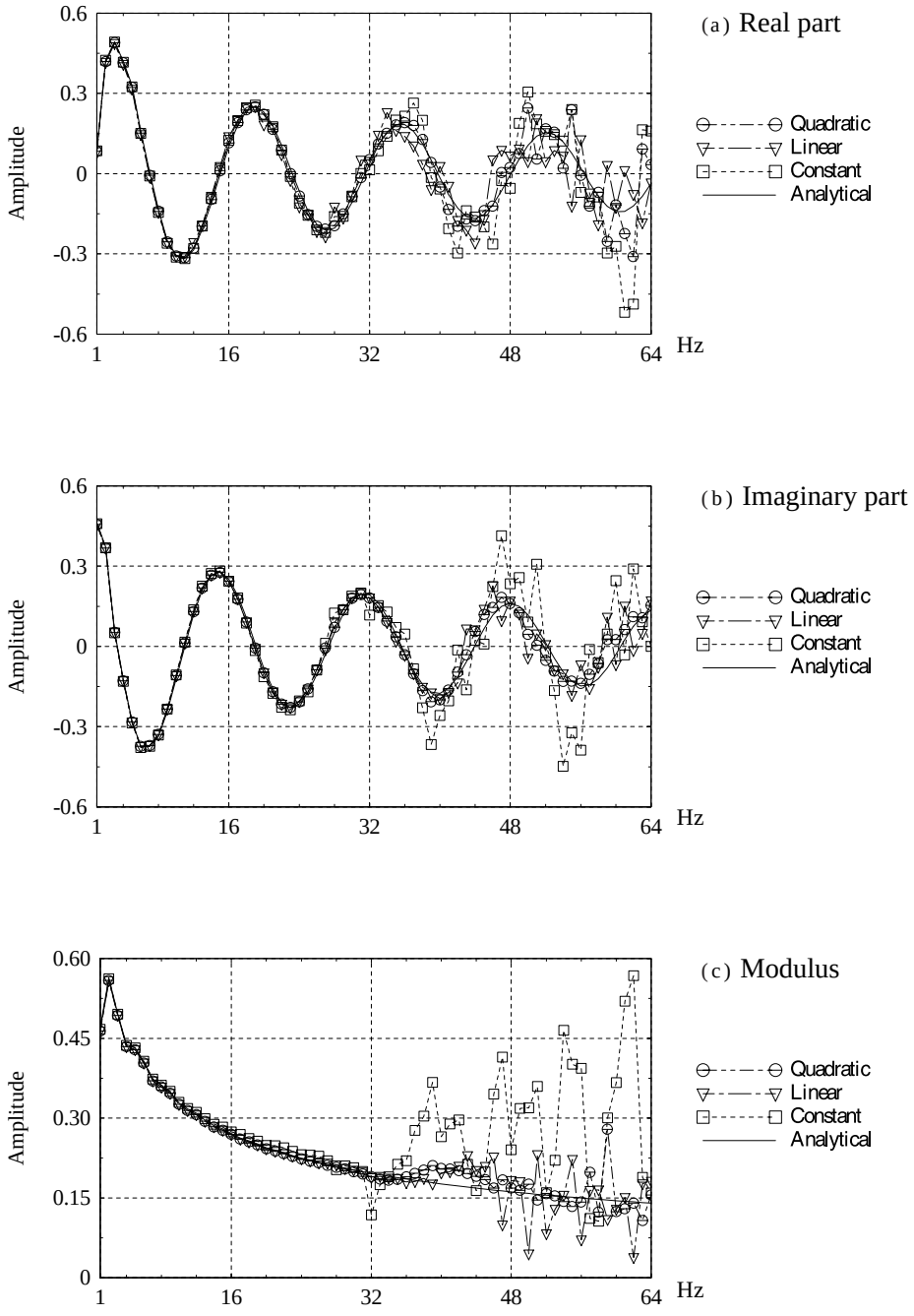

Fig. 7. Anti-plane field scattered by a cylindrical cavity modelled with 25 boundary elements.

6. Conclusions

This paper presented exact expressions for the singular integrals involved in the application of the BEM method to problems of wave diffraction in anti-plane shear wave motion (or acoustic waves in a fluid medium). These expressions were then compared with those obtained by the purely numerical method in current use, which allowed an assessment of the accuracy of the latter for a broad range of frequencies. The method was next applied to ideal examples of wave scattering by elastic inclusions modelled with constant, linear and quadratic elements, which permitted evaluating the accuracy of the BEM formulation against the theoretical solutions available for these problems.

It was first observed that an evaluation of the singular integrals by numerical quadrature requires at least four Gauss–Legendre stations for acceptable accuracy. From the examples presented, it was then seen that the response improved and approached the exact solution as the expansion order and the number of boundary elements used was

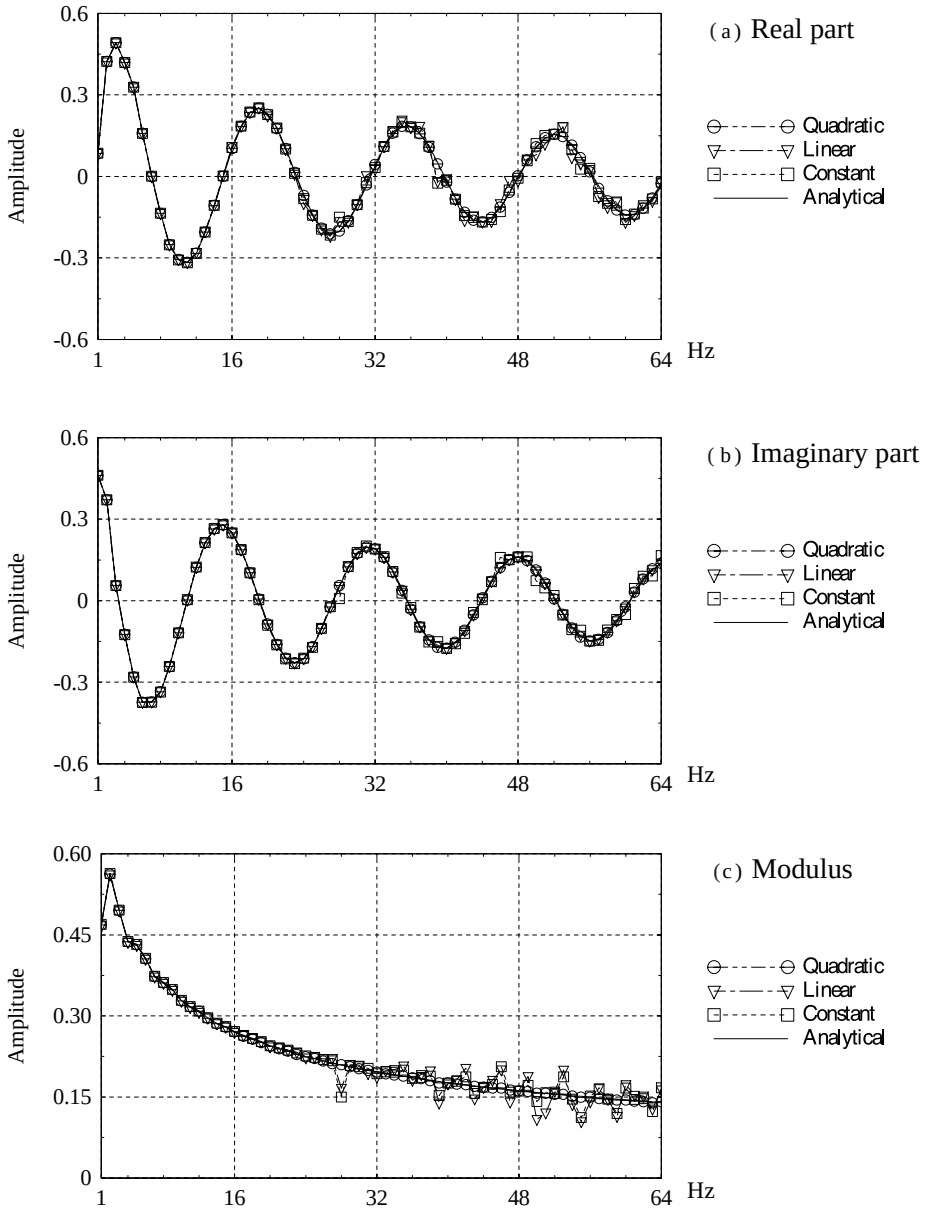

Fig. 8. Anti-plane field scattered by a cylindrical cavity modelled with 50 boundary elements.

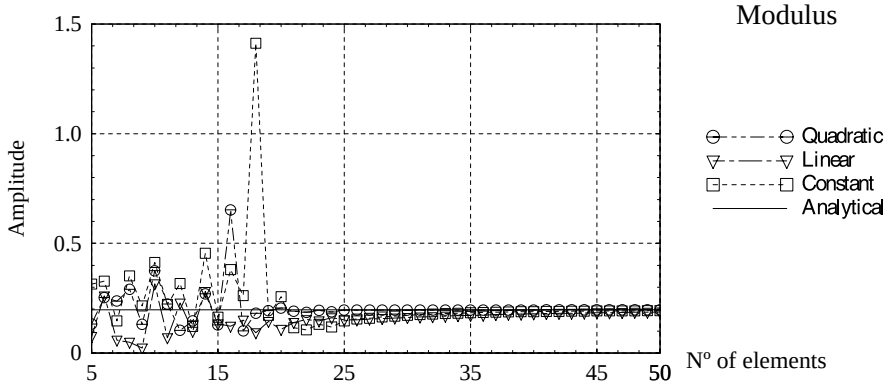

Fig. 9. Anti-plane field scattered by a cylindrical cavity in presence of an harmonic excitation source of 32 Hz.

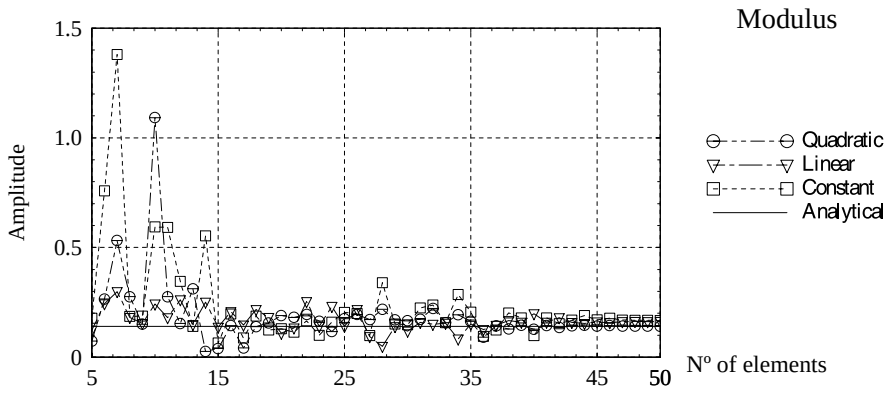

Fig. 10. Anti-plane field scattered by a cylindrical cavity in the presence of an harmonic excitation source of 64 Hz.

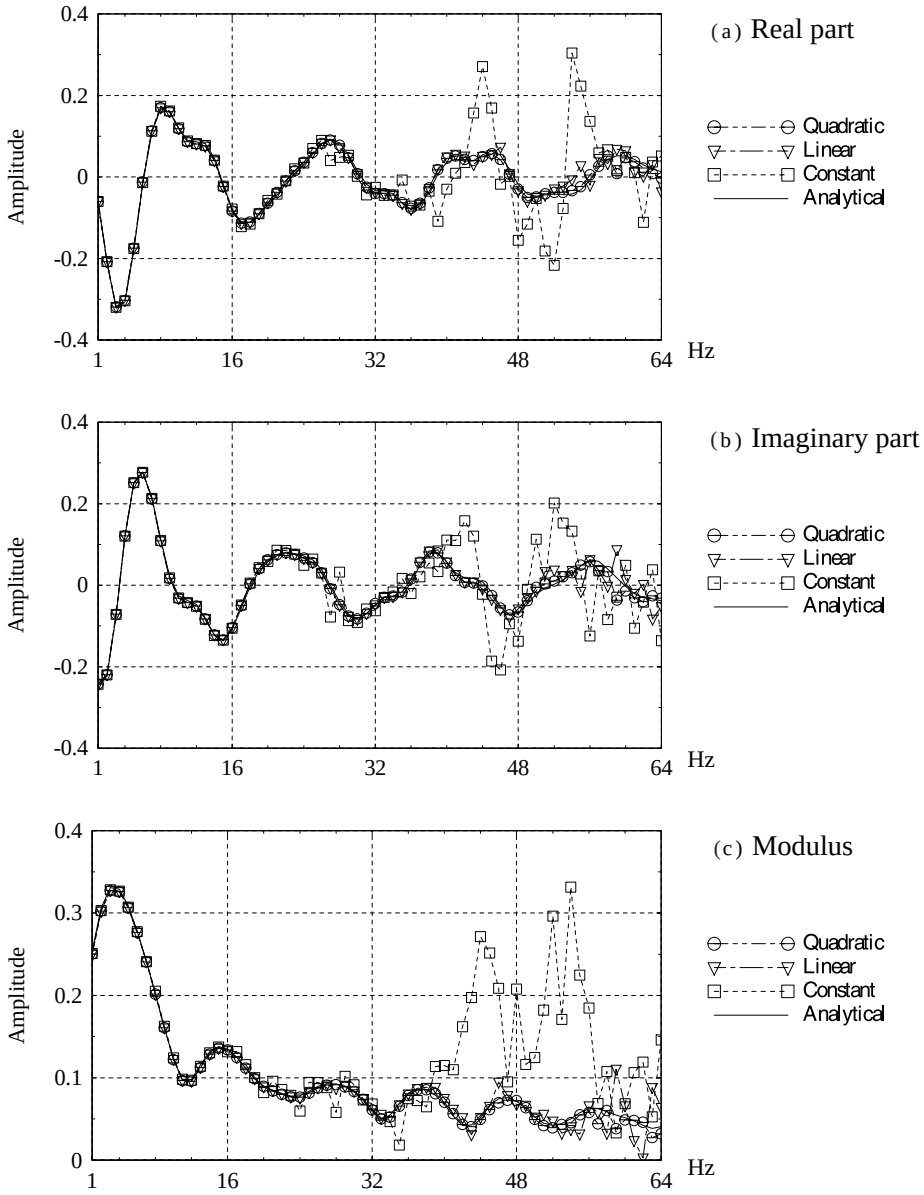

Fig. 11. Anti-plane field scattered by a cylindrical elastic inclusion modelled with 25 boundary elements.

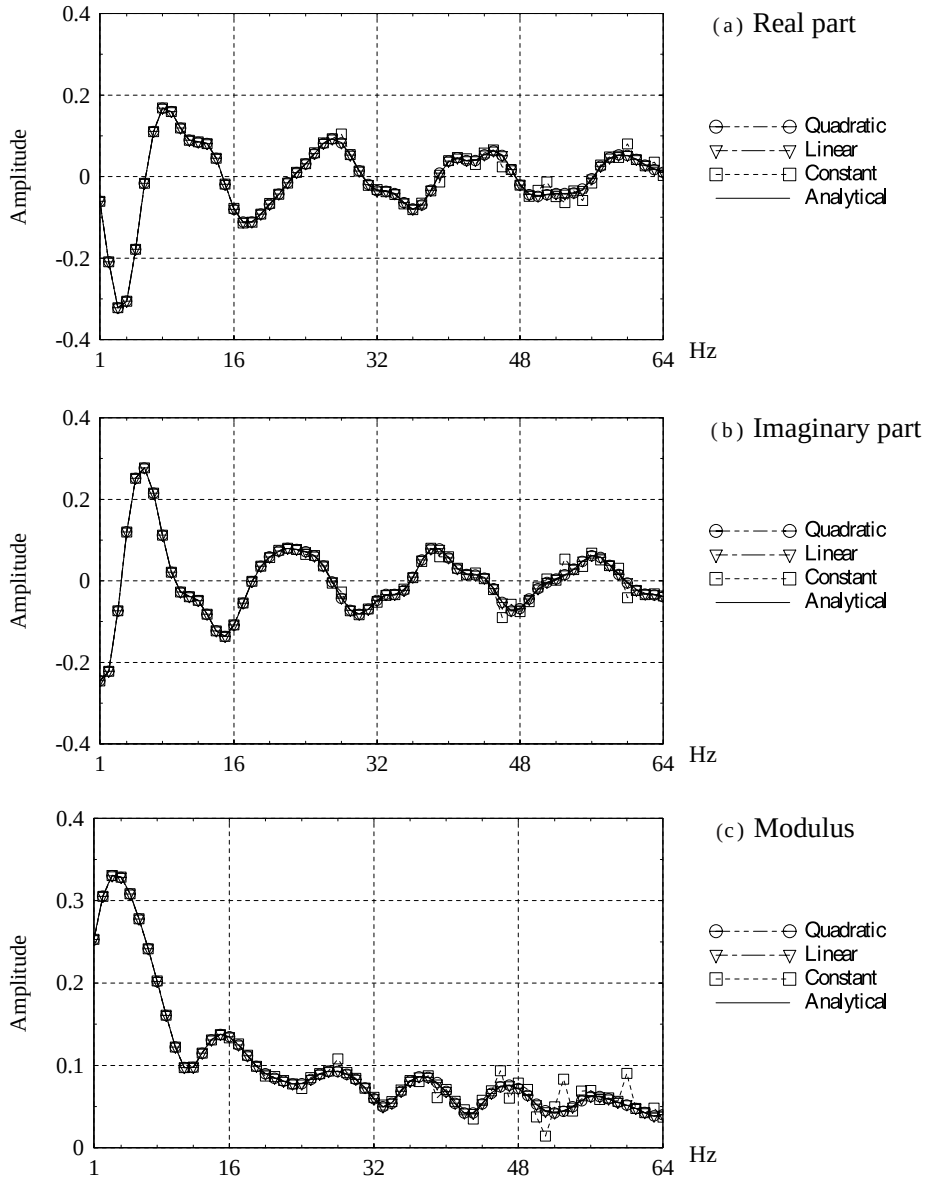

Fig. 12. Anti-plane field scattered by a cylindrical elastic inclusion modelled with 50 boundary elements.

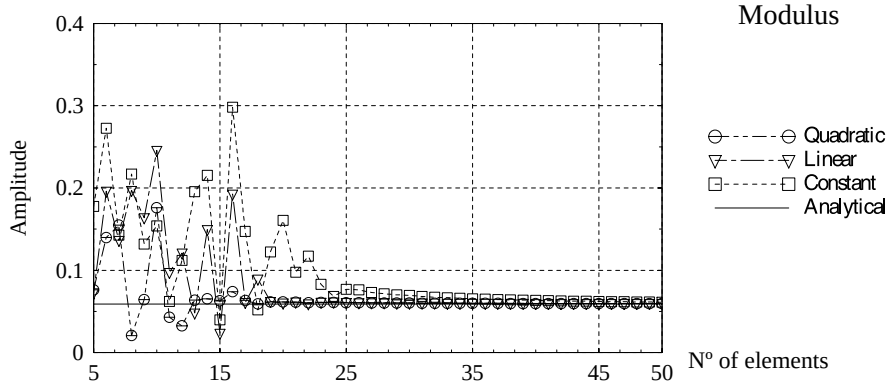

Fig. 13. Anti-plane field scattered by a cylindrical elastic inclusion in presence of a harmonic excitation source of 32 Hz.

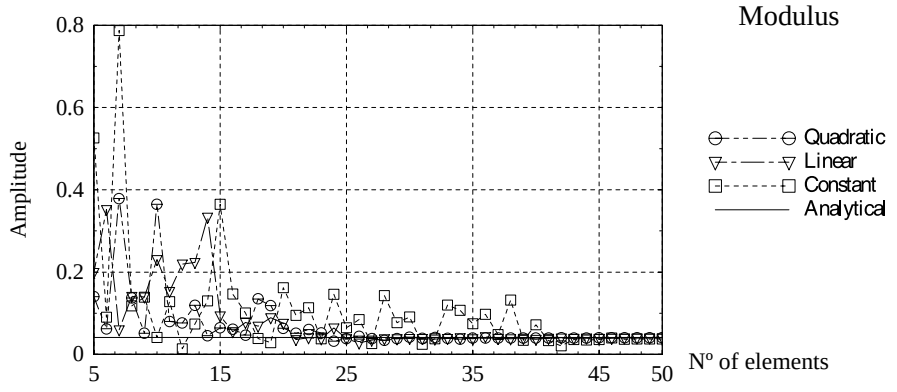

Fig. 14. Anti-plane field scattered by a cylindrical elastic inclusion in the presence of a harmonic excitation source of 64 Hz.

increased. This expected finding provided confirmation that the integrals presented herein are both accurate and valid.

References

[1] Wong HL, Trifunac MD. Surface motion of a semi-elliptical alluvial valley for incident plane SH-waves. Bull Seismic Soc Am 1974;64:1389–403.

[2] Lee VW, Karl JA. Diffraction of SV waves by underground circular, cylindrical cavities. Soil Dynamics Earthquake Engng 1992;11:445–56.

[3] Lee VW, Wu X. Application of the weighted residual method to diffraction by 2D canyons of arbitrary shape: II incident P, SV and Rayleigh waves. Soil Dynamics Earthquake Engng 1994;13:365–75.

[4] Kausel E. Forced vibrations of circular foundations in layered media. MIT Research Report 74-11. Department of Civil Engineering, Massachusetts Institute of Technology, Cambridge, Massachusetts, 1974.

[5] Sanchez-Sesma FJ. Site effects on strong ground motion. Soil Dynamics Earthquake Engng 1987;6:124–32.

[6] Dravinski M, Mossessian TK. Scattering of plane harmonic P, SV and Rayleigh waves by dipping layers of arbitrary shape. Bull Seismic Soc Am 1987;77:212–35.

[7] Pedersen HA, Sanchez-Sesma FJ, Campillo M. Three-dimensional scattering by two-dimensional topographies. Bull Seismic Soc Am 1994;84:1169–83.

[8] Beskos DE. Wave propagation through ground. In: Manolis GD, Davies TG, editors. Boundary element techniques in geomechanics, Southampton and Oxford: Computational Mechanics Publications and Elsevier, 1993. p. 359.

[9] Hall WS. Integration methods for singular boundary element integrands. In: Brebbia CA, editor. Boundary elements X, 1. Southampton: Computational Mechanics Publications, 1989. p. 219.

[10] Kawase H. Time-domain response of a semi-circular canyon for incident SV, P and Rayleigh waves calculated by the discrete wavenumber boundary element method. Bull Seismic Soc Am 1988;78:1415–37.

[11] Tadeu AJB, Kausel E, Vrettos C. Modelling and seismic imaging of buried structures. Soil Dynamics Earthquake Engng 1996;15:387–97.

[12] Tadeu AJB. Modelling and seismic imaging of buried structures. PhD thesis. M.I.T., Department of Civil Engineering, Cambridge, Massachusetts, 1992.

[13] Pao YH, Mow CC. Diffraction of elastic waves and dynamic stress concentrations, Crane and Russak, 1973.

[14] Manolis GD, Beskos DE. Boundary element methods in elastodynamics, Unwin Hyman, 1988.

[15] Tadeu AJB, Santos PFA. Performance of higher order elements in the analysis of a two-dimensional acoustic medium. BEM 21, Oxford, UK, 1999.

[16] Abramowitz M, Stegun IA. Handbook of mathematical functions, New York: Dover, 1964. p. 480–4.